Materials and Design 177 (2019) 107851

Contents lists available at ScienceDirect

Materials and Design

journal homepage: www.elsevier.com/locate/matdes

Improving the electrochemical performance of Si-based anode via gradient Si concentration

Zhenbin Guo [a,b], Limin Zhou [b], Haimin Yao [a,b,*]

[a] The Hong Kong Polytechnic University Shenzhen Research Institute, Shenzhen 518057, China
[b] Department of Mechanical Engineering, The Hong Kong Polytechnic University, Hong Hum, Kowloon, Hong Kong

HIGHLIGHTS

- The graded electrodes exhibited superior performance (1299 mAh g^{-1} after 50 cycles) than that of the homogeneous ones.
- The optimal structural designs for the two- and three-layer graded electrodes were determined.
- The delamination problem between the current collector and Si-based electrode film was solved in the graded electrodes.
- The concept of graded electrode can be applied to the other anode materials suffering from the large-volume-change problem.

GRAPHICAL ABSTRACT

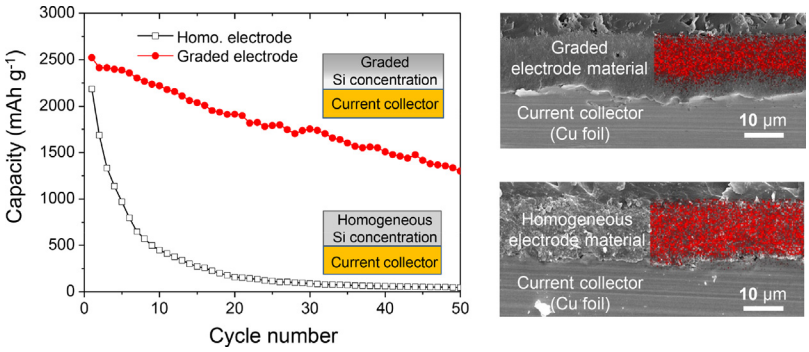

ARTICLE INFO

Article history:
Received 20 February 2019
Received in revised form 10 May 2019
Accepted 11 May 2019
Available online 14 May 2019

Keywords:
Delamination
Functionally graded materials
Energy materials
Heterogeneity
Lithium-ion batteries

ABSTRACT

Silicon (Si) has long been regarded as one of the most promising anode materials for the next-generation lithium-ion batteries (LIBs) due to its exceptional specific capacity and apt working voltage. However, the drastic volume change of Si during lithiation/delithiation processes tends to cause various mechanical failure problems including the delamination between current collector and electrode materials, resulting in poor stability and degradation of LIBs. Inspired by the functional graded design in natural biomaterials, we propose to solve the interfacial delamination problem by reallocating the Si in the electrode in a graded manner. The prepared graded electrodes especially those after gradient optimization are found quite successful in alleviating the interfacial delamination, resulting in higher capacity and capacity retention, higher coulombic efficiency, higher effective mass loading in comparison to the traditional ones. Specifically, the optimal graded electrode shows a charge capacity of 1299 mAh g^{-1} after 50 cycles, which is much higher than that of the homogeneous electrode (66 mAh g^{-1}). Such a graded electrode can be easily implemented by existing manufacturing techniques and synergize with other strategies for solving the large-volume-change problem of Si. Our work provides a guideline for the design and manufacture of the graded Si-based electrodes for LIBs.

1. Introduction

The rapid development of emerging industries such as electric automobile and wearable electronics makes higher demands on capacity

* Corresponding author at: The Hong Kong Polytechnic University Shenzhen Research Institute, Shenzhen 518057, China.
E-mail address: mmhyao@polyu.edu.hk (H. Yao).

https://doi.org/10.1016/j.matdes.2019.107851

and durability of the power supplies. Lithium-ion batteries (LIBs), one of the most prevalent devices for energy storage, have long been anticipated to cater for such demands since its advent in 1990 [1,2]. For LIBs, however, high capacity and high cycling performance seem two conflicting attributes that can be hardly achieved together [3–5]. For example, the carbon-based LIBs exhibit satisfactory cycling performance while their capacity is capped by 372 mA h g^{-1}, the theoretical capacity of carbon. In contrast, the capacity of silicon-based LIBs, in theory, can reach as high as 4200 mA h g^{-1}. Unfortunately, they suffer from poor cyclability caused by the huge volume change (300–400%) of Si during the process of lithiation and delithiation [6–8]. To make the best use of the high capacity of Si and meanwhile avoid the problems caused by large volume change, a lot of efforts have been made from different angles [9–12]. For example, study on the size effect of lithiation of Si nanoparticles indicated that the lithiation-induced fracture of Si does not happen if the size of Si particle is reduced to below a critical value around ~150 nm in diameter, implying that size reduction is an effective way to avoid pulverization of Si particles [13]. However, size reduction does not genuinely refrain the ratio of volume change of Si particles. To constrain the volume change of Si, external coating such as carbon shell was applied and found effective in promoting the electrochemical performance of LIBs [14–17]. Recently, yolk-shell structured Si nanoparticles and hollow Si nanoparticles were developed, which were found to improve the cyclability of Si-based LIBs further [18–20]. These innovative structurized Si nanoparticles provided a promising avenue for solving the large volume change problem of Si, but their high cost and complex fabrication process greatly hinder their wide application in industries. Nowadays, it remains practically meaningful to seek facile solutions which are applicable to plain Si materials and mass production. Here, we attempt the drastic volume change problem of Si from a different angle. Rather than modifying the structure of Si nanoparticles, we still stick to the plain Si nanoparticles but introduce a variation of their distribution in space.

Traditionally, Si-based anode of LIB is produced by blending Si nanoparticles, conductive additive (e.g., carbon black) and binder (e.g., polyvinylidene fluoride) with solvent (e.g., N-Methyl-2-pyrrolidone). The obtained slurry is cast on a current collector (e.g., copper foil) and dried for use. In that case, the concentration of Si nanoparticles has little variation in the film of anode material. Upon lithiation, the anode would swell uniformly, resulting in strain misfit between the anode material and current collector, and interfacial stress is developed consequently. Such stress is normally shear-dominant and highly concentrated at the edge of the contact area and therefore prone to initiate crack and delamination of the interface, leading to poor contact between the anode material and current collector and subsequent degradation of the electrochemical performance. To suppress the delamination of the interface between the Si-based electrode material and current collector, application of functionally graded materials (FGMs) is believed a feasible approach as they have been demonstrated capable of enhancing the resistance to contact and impact damages and adhesion strength [21–25]. Studies on biological materials indicated that FGMs are also widely adopted in nature to mitigate the stress concentration possibly taking place on the interfaces in natural laminated composites [26–28]. Recently, the concept of FGM started to be applied to the design of energy materials [29–33]. It was found that FGMs help in reducing the transport barrier of charge carriers in electrodes [31–33]. Inspired by these successes of FGMs, here we propose to address the interfacial delamination problem of Si by using functionally layer-graded electrodes. First, we experimentally demonstrate the merits of graded electrodes over the traditional homogenous counterparts. Then, the structural designs of the graded electrodes are further optimized to achieve the best improvement of performance as compared to those of the homogeneous controls.

2. Experimental procedure

2.1. Preparation of homogeneous electrodes as controls

Si nanoparticles (Si NPs), carbon black (CB) and polyvinylidene fluoride (PVDF) in a mass ratio of 3:1:1 is mixed sufficiently with solvent N-Methyl-2-pyrrolidone (NMP) using pestle and mortar. A 100 μm thick layer of the obtained slurry is cast onto a copper foil (15 cm × 10 cm × 15 μm) with a film applicator and then dried at 80 °C for 3 h and subsequently 120 °C for 10 h in a vacuum oven. The dried electrode film together with the copper foil substrate is then cut into circular disk-like electrodes with a punch cutter. The mass of electrodes is measured, from which the areal mass loadings of Si, CB, and PVDF are calculated to be m_{Si}^{HO}=0.744 g cm^{-2}, m_{CB}^{HO}=0.248 g cm^{-2}, and m_{PVDF}^{HO}=0.248 g cm^{-2}, respectively. Here, areal mass loading refers to the mass of the electrode constituents (e.g., Si NPs, CB and PVDF) deposited on the current collector per unit area. For a sensible comparison, the same areal mass loadings are maintained in the corresponding graded electrodes.

2.2. Preparation of two-layer graded electrodes

The two-layer graded electrodes are fabricated through a two-step casting process. To prepare the Si-free transition layer, first CB and PVDF in a mass ratio of 1:1 is mixed with solvent NMP using pestle and mortar. The obtained slurry is cast onto a copper foil (15 cm × 10 cm × 15 μm) with a film applicator and then dried at 80 °C for 3 h. The areal loadings of constituents CB and PVDF in the transition layer, which depends on the clearance of the applicator and the amount of solvent NMP used, can be estimated from the weight of a piece of sample cut from the specimen. Then, the slurry of the Si-rich layer is prepared by blending Si NPs, CB and PVDF in a mass ratio of m_{Si}^{HO}: $m_{CB}^{HO} - m_{CB}^{TR}$: $m_{PVDF}^{HO} - m_{PVDF}^{TR}$ with certain amount of solvent NMP, where m_{Si}^{HO}, m_{CB}^{HO}, m_{PVDF}^{HO} stand for the areal loadings of Si, CB and PVDF in the homogeneous control, and m_{CB}^{TR} and m_{PVDF}^{TR} refer to the areal loadings of CB and PVDF in the transition layer that has been fabricated. Likewise, the obtained slurry is then cast onto the transition layer attached on the Cu foil using a film applicator. Here a proper clearance of the applicator should be chosen to ensure that the total areal loading of each ingredient in the two-layer electrode obtained is the same as that in the homogeneous control. After drying at 80 °C for 3 h and subsequently 120 °C for 10 h in a vacuum oven, two-layer graded electrodes are obtained by cutting the specimen with a circular punch cutter.

2.3. Preparation of three-layer graded electrodes

The three-layer graded electrodes are fabricated through a three-step casting process. First, a Si-free transition layer is coated on a copper foil as shown above for the two-layer graded electrode. The areal loading of CB and PVDF in the transition layer, m_{CB}^{TR} and m_{PVDF}^{TR}, are estimated from the weight of a piece of sample cut from the specimen. Then, the slurry for the first Si-rich sublayer is prepared by mixing Si NPs, CB and PVDF in a mass ratio of C_1:(100 − C_1)/2:(100 − C_1)/2 with solvent NMP using pestle and mortar, so that the Si concentration of C_1 wt% can be achieved. Likewise, the obtained slurry is cast onto the translation layer using a film applicator with a clearance of 50 μm and then dried at 80 °C for 3 h. The areal loading of Si NPs, CB and PVDF in the first Si-containing sublayer, designated as $m_{Si}^{(1)}$, $m_{CB}^{(1)}$ and $m_{PVDF}^{(1)}$, are determined from the measured mass of this sublayer and the known mass ratio. Then the slurry of the second Si-containing sublayer is prepared by mixing Si NPs, CB and PVDF in a mass ratio of $m_{Si}^{HO} - m_{Si}^{(1)}$: $m_{CB}^{HO} - m_{CB}^{TR} - m_{CB}^{(1)}$: $m_{PVDF}^{HO} - m_{PVDF}^{TR} - m_{PVDF}^{(1)}$ with certain solvent NMP, resulting in Si concentration of $\frac{m_{Si}^{HO} - m_{Si}^{(1)}}{m_{Si}^{HO} - m_{Si}^{(1)} + m_{CB}^{HO} - m_{CB}^{TR} - m_{CB}^{(1)} + m_{PVDF}^{HO} - m_{PVDF}^{TR} - m_{PVDF}^{(1)}} \times 100\%$, which is designated as C_2%. Likewise, the obtained slurry is then cast onto the

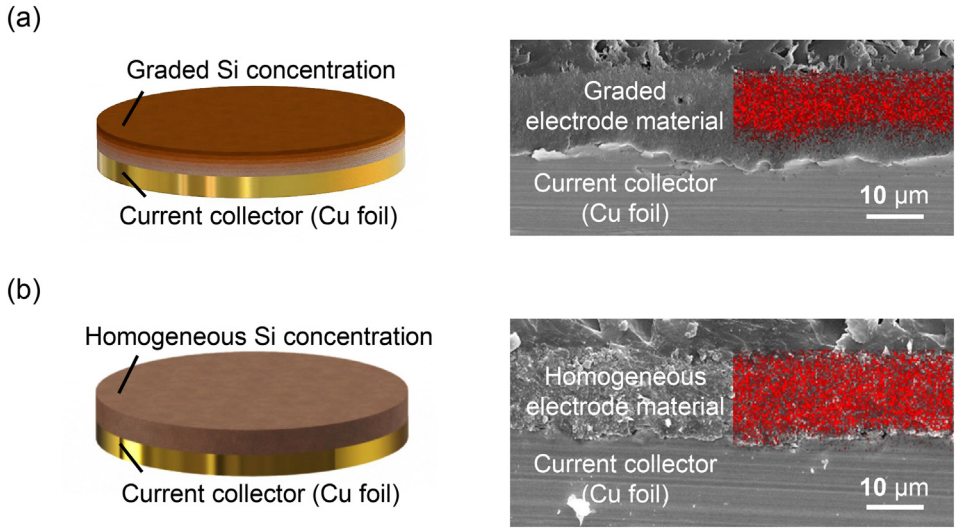

Fig. 1. Schematics and the cross-sectional energy-dispersive X-ray spectroscopy (EDS) mapping of Si element for (a) graded and (b) homogeneous Si-based electrodes.

first sublayer using a film applicator. Here a proper clearance of the applicator should be chosen to ensure that the total areal loading of each constituent in the three-layer electrode obtained is the same as that in the homogeneous control. After drying at 80 °C for 3 h and subsequently 120 °C for 10 h in a vacuum oven, three-layer graded electrodes are obtained by cutting the specimen with a circular punch cutter.

2.4. Microstructure characterization

Scanning electron microscopy (SEM) and energy-dispersive X-ray spectroscopy (EDS) measurements are conducted on a Tescan VEGA3 scanning electron microscope equipped with backscattered electron diffraction (BSE) and energy dispersive X-ray spectroscopy detector.

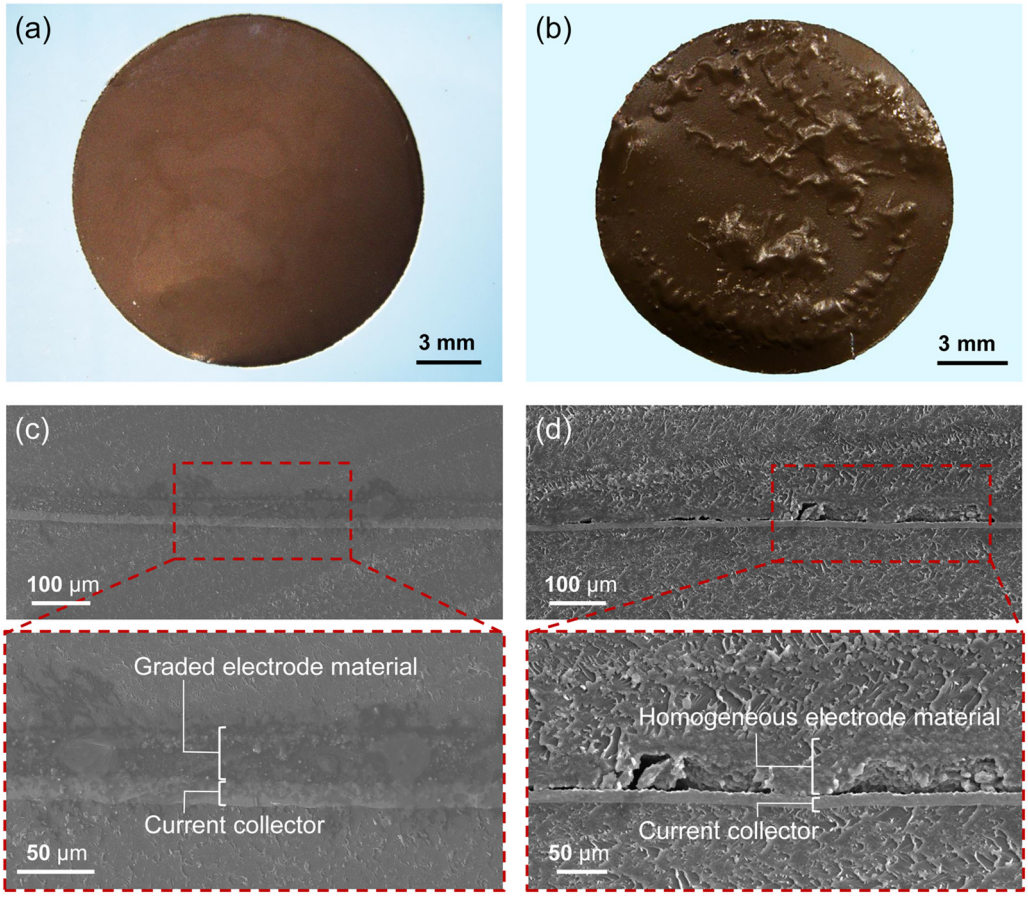

Fig. 2. Surface morphologies of (a) graded and (b) homogeneous Si-based electrodes and cross-section of (c) graded and (d) homogeneous Si-based electrodes after 500 discharge/charge cycles at voltage between 0.01 V and 1.2 V vs. Li/Li^+ and rate of 0.05C.

2.5. Battery construction and electrochemical characterizations

Electrochemical performances are characterized using CR2032 coin-type half-cells. Lithium foil is employed as the counter electrode and Celgard 2400 is adopted as the separator. The as-prepared electrode is assembled into a half-cell in an ultra-pure argon-filled glove box (<0.5 ppm of oxygen and water) using 1 M $LiPF_6$ in ethylene carbonate and diethyl carbonate (EC:DEC = 1:1) with a 5 vol% fluoroethylene carbonate (FEC) and 1 vol% vinylene carbonate (VC) additive as the electrolyte. Galvanostatic discharge/charge test is carried out on a LAND CT-2001A at the potential ranging from 0.01 to 1.2 V vs. Li^+/Li. Electrochemical impedance spectroscopy (EIS) experiments are performed on an electrochemical workstation P4000 over the frequency ranging from 100 kHz to 10 MHz with an amplitude of 5 mV. All electrochemical cycling measurements are carried out at room temperature. All the specific capacities and current density are assessed based on the weight of Si.

3. Results and discussion

Fig. 1 shows the X-ray spectroscopy mapping of Si element (red dots) collected from the cross-section of the graded electrode in comparison to that from the homogeneous control. As expected, a stepwise two-leveled Si concentration is successfully achieved in the graded electrode (Fig. 1a), while the distribution of Si in the control is much more uniform (Fig. 1b).

The as-prepared graded electrodes, as well as the homogeneous ones, are installed into coin-type half-cells for the characterization of the electrochemical performance. After enough discharge/charge cycles, some randomly selected cells are dissembled to examine the status of the electrodes. Fig. 2 compares the morphologies between a typical graded electrode and a homogeneous control after 500 cycles. The surface of the graded electrode seems intact and flat (see Fig. 2a), implying that the electrode layer remains firmly attached on the current collector

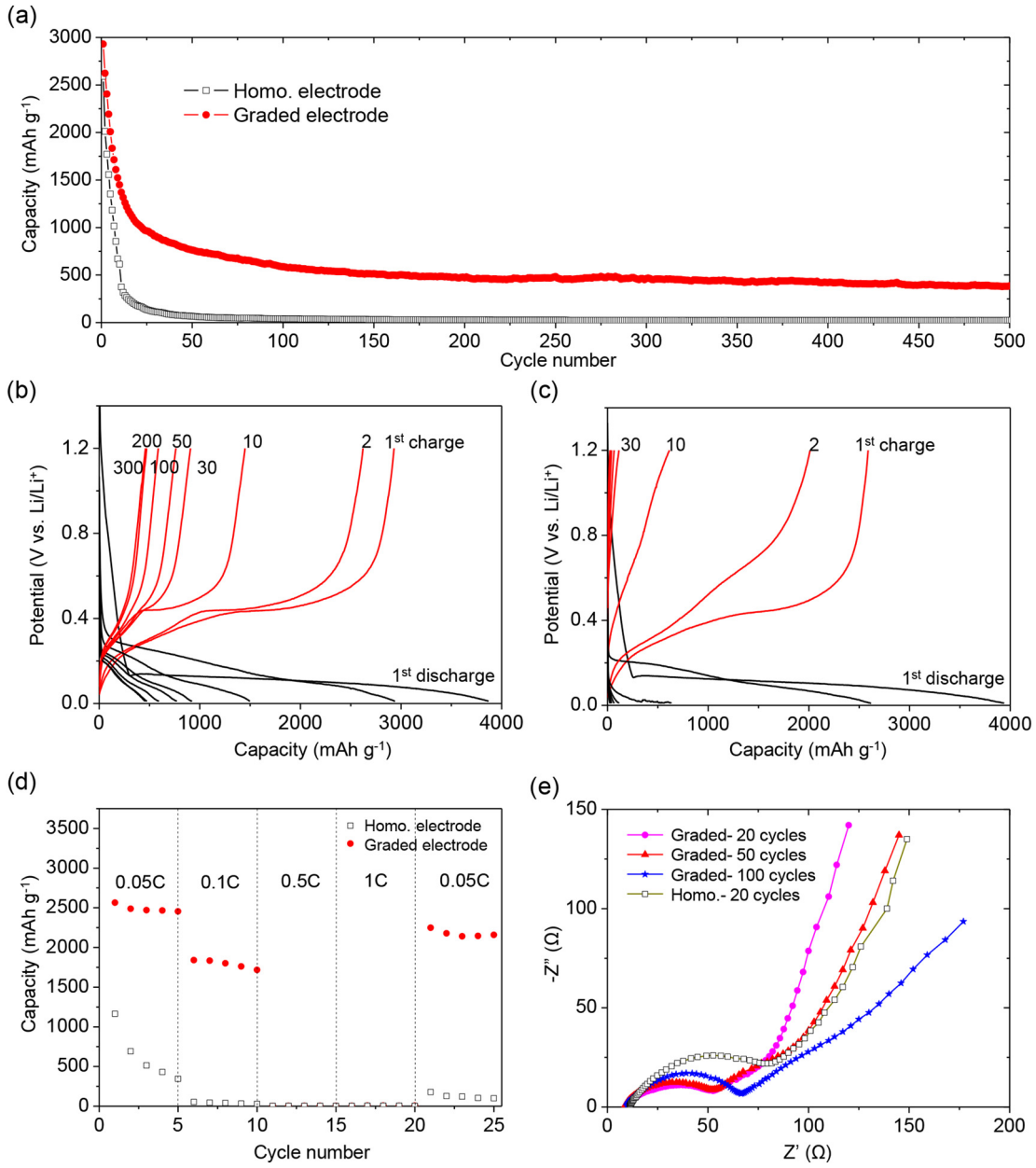

Fig. 3. Electrochemical tests for a two-layer graded electrode with transition layer thickness being 25 μm and homogeneous control. (a) Cycling performance at a voltage from 0.01 to 1.2 V vs. Li/Li^+ and a rate of 0.05C. (b-c) Galvanostatic discharge/charge profiles for graded and homogeneous electrode respectively at a rate of 0.05C. (d) Rate capability tests. (e) Nyquist plots at selected cycles.

and no delamination has taken place in between (see Fig. 2c). In contrast, on the surface of the homogeneous counterpart, bubbling structures have already been developed (see Fig. 2b), implying the advent of severe interface delamination between the electrode film and the current collector (see Fig. 2d).

Due to such superior structural integrity shown above, the graded electrode exhibits much better electrochemical performances. Fig. 3a compares the cycling performance of the graded electrode and homogeneous electrode. Clearly, the graded electrode exhibits overwhelming advantages over the homogeneous one in manifesting the superior capacity of Si. In particular, the graded electrode shows a charge capacity of 2930 mA h g^{-1} at the 1st cycle and 390 mA h g^{-1} after 500 cycles. Such high capacity of the graded electrode overpasses those of Si-based electrodes using superior binders such as carboxymethyl cellulose and sodium alginate [34]. For the homogeneous electrode, albeit its initial charge capacity reaches 2589 mA h g^{-1}, it almost fades away (66 mA h g^{-1}) after 50 cycles or so. Such poor cyclability should be attributed to the delamination of the electrode layer from the current collector as shown in Fig. 2.

Fig. 3b and c show the galvanostatic discharge/charge profiles of the graded and homogeneous electrodes cycled at the voltage range of 0.01–1.20 V and rate of 0.05C (i.e., 210 mA g^{-1}). When Li-ions get inserted into the graded electrode for the first time (discharging process), the voltage drops drastically to 0.14 V, followed by a steady plateau and then a progressive decrease to 0.01 V. During the ensuing charging (delithiation) process, the voltage initially increases quickly, followed by a relatively steady plateau ranging from 0.25 V to 0.50 V. Similar plateaus can be observed even after 300 cycles for the graded electrode, implying a stable voltage window for charging and discharging. In contrast, for the homogeneous electrode, voltage plateau is only observed in the first a few cycles and disappears after 10 cycles. Moreover, it can be calculated from Fig. 3b and c that the initial coulombic efficiency of the graded electrode is 76%, which is higher than that of the homogeneous electrode, namely 66%, implying that the Si in the graded electrode has been utilized in a more efficient way. Fig. 3d compares the rate capability between the graded electrode and the homogeneous one. At the same discharge/charge rate varying from 0.05C to 1C, the graded electrode always delivers higher capacities than the homogeneous one does. As the rate returns to 0.05C, the graded anode exhibits >80% capacity retention, which is much higher than that of the homogeneous electrode namely 2%, implying the superior sustainability of the graded design. To further understand the effect of graded Si concentration on the electrochemical performance of LIB, impedance spectroscopy measurements were carried out. Fig. 3e compares the Nyquist plots of the graded and homogeneous electrodes at selected cycles, each of which consists of a depressed semicircle at high frequencies and a straight line at low frequencies. The diameters of the high-frequency semicircles of the graded electrode, which represent the solid-electrolyte interphase (SEI) resistance including electrical and ionic resistances, are apparently smaller than that of the homogeneous one even after 100 cycles. This indicates that the SEI layer in the graded electrode, compared to that of the homogeneous one, is less resistant to the transfer of electrons and Li-ions.

To make the best use of the graded strategy, the thickness effect of the transition layer on the capacity is studied. Fig. 4a compares the specific charge capacity of graded electrodes with different transition layer thicknesses (H_c). All electrodes shown in Fig. 4a contain the same amounts of constituents including Si NPs, CB and PVDF. The only difference between them is the distribution of these constituents in space. Fig. 4a indicates that the capacity of a two-layer electrode is maximized when the thickness of the transition layer takes 25 μm or so. Such optimal two-layer graded electrode shows a stable charge capacity of 1263 mA h g^{-1} after 20 cycles, which is more than four times higher than that of the homogeneous electrode. A detailed illustration of the thickness effect of the transition layer on the cycling performance is shown by Fig. 4b. Actually, the electrochemical performance shown in Fig. 3 pertains to a graded electrode with transition layer thickness equal to 25 μm. The existence of such optimal thickness of the transition layer may be attributed to the fact that thick Si-free transition layer would lead to the high concentration of Si on the top of it as the mass loading of Si is maintained the same. Overconcentrated Si will cause severe volume change, delamination between the transition layer and Si-containing layer, and degradation of the electrochemical performance.

In addition to improving the electrochemical performance, graded Si concentration also helps to enhance the effective mass loading of the electrode. Fig. 5a shows the evolution of initial areal capacity with the increase of the areal mass loading of Si, which is achieved by thickening the Si-rich layer. It is surprising to notice that higher mass loading of Si may not always give rise to a higher capacity. There is a saturating point, beyond which addition of Si will bring limited or even negative increment on the areal capacity. For the graded electrode, such saturation of capacity occurs as the areal mass loading of Si reaches 1.8 mg cm^{-2}, which is much higher than that of the homogeneous electrode namely 1.1 mg cm^{-2}. For a two-layer graded electrode with optimally thick transition layer (25 μm), the maximum areal capacity (charge) that can be achieved is 4.64 mA h cm^{-2} which is almost twice as large as that of a homogeneous electrode with the same mass loading of Si. This indicates that the utilizing efficiency of Si can be greatly improved simply by redistributing the Si NPs in space. Fig. 5b compares the cycling performance of graded and homogeneous electrodes with comparable areal loading of Si. As expected, the graded electrodes exhibit much better cycling performance in comparison with the homogeneous ones.

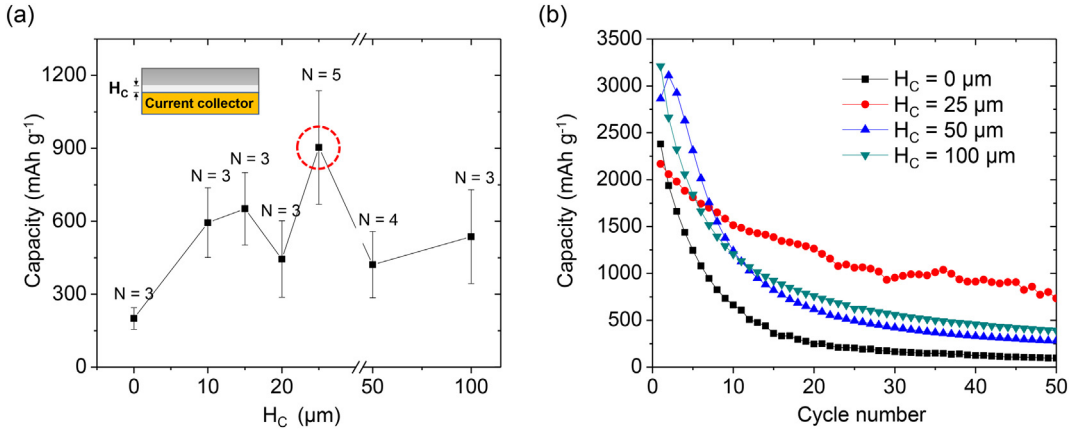

Fig. 4. (a) Comparison of the capacity (at the 20th cycle) achieved by graded electrodes with a transition layer of different thicknesses (H_c). Here, H_c refers to the thickness of the transition layer before drying, N is the number of tested cells and the error bar represents the standard deviation of the results obtained from N battery cells. (b) The charge capacity of the two-layer electrodes with different H_c during cycling test at the voltage between 0.01 V and 1.2 V vs. Li/Li^+ and a rate of 0.05C.

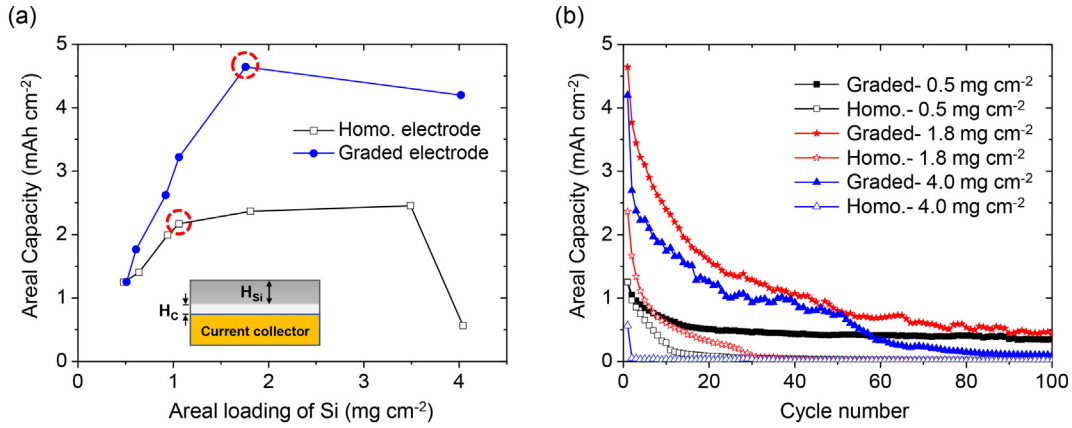

Fig. 5. (a) Evolution of the areal capacity (charge) with the areal loading of Si. (b) Electrochemical performance of graded and homogeneous Si-based electrodes with different areal loading of Si at a voltage between 0.01 V and 1.2 V vs. Li/Li^+ and a rate of 0.05C.

More specifically, the areal capacity of all the homogeneous electrodes fades away after 30 cycles or even less, irrespective of the areal loading of Si, while the graded electrodes especially that with Si mass loading of 1.8 mg cm^{-2} maintains a considerable areal capacity even after 100 cycles.

The success of a two-layer graded electrode in improving the performance of LIB motivates the exploitation of further potential of the graded design. For this purpose, we further divide the Si-rich layer into two finer sublayers with Si concentrations designated as C_1 wt% and C_2 wt%, respectively (see the inset of Fig. 6 for schematics). The ratio of C_1/C_2 characterizes the gradient of the Si concentration along the thickness direction. $C_1/C_2 < 1$ refers to the cases with Si concentration monotonically ascending along with the thickness outwards; $C_1/C_2 > 1$ stands for the cases with Si more concentrated inside the electrode than outside. When $C_1/C_2 = 1$, it reduces to the two-level graded electrode as discussed above. For a sensible comparison, the amount of each constituent applied in all the three-layer electrodes, including Si NPs, CB and PVDF, is kept the same. The dependence of the charge capacity on the ratio of C_1/C_2 is shown in Fig. 6a. The highest capacity (1299 mA h g^{-1} after 50 cycles) of the three-layer electrode is achieved when $C_1/C_2 \cong 0.57$. The corresponding cycling performance is shown in Fig. 6b compared to those of the electrodes with C_1/C_2 greater and smaller than 0.57. Despite the large volume change after cycling, which can be seen from the increase of the electrode film thickness from 13.5 ± 0.2 μm to 19.0 ± 0.5 μm, no delamination is observed on the interface with the current collector, as shown in Fig. 6c and d.

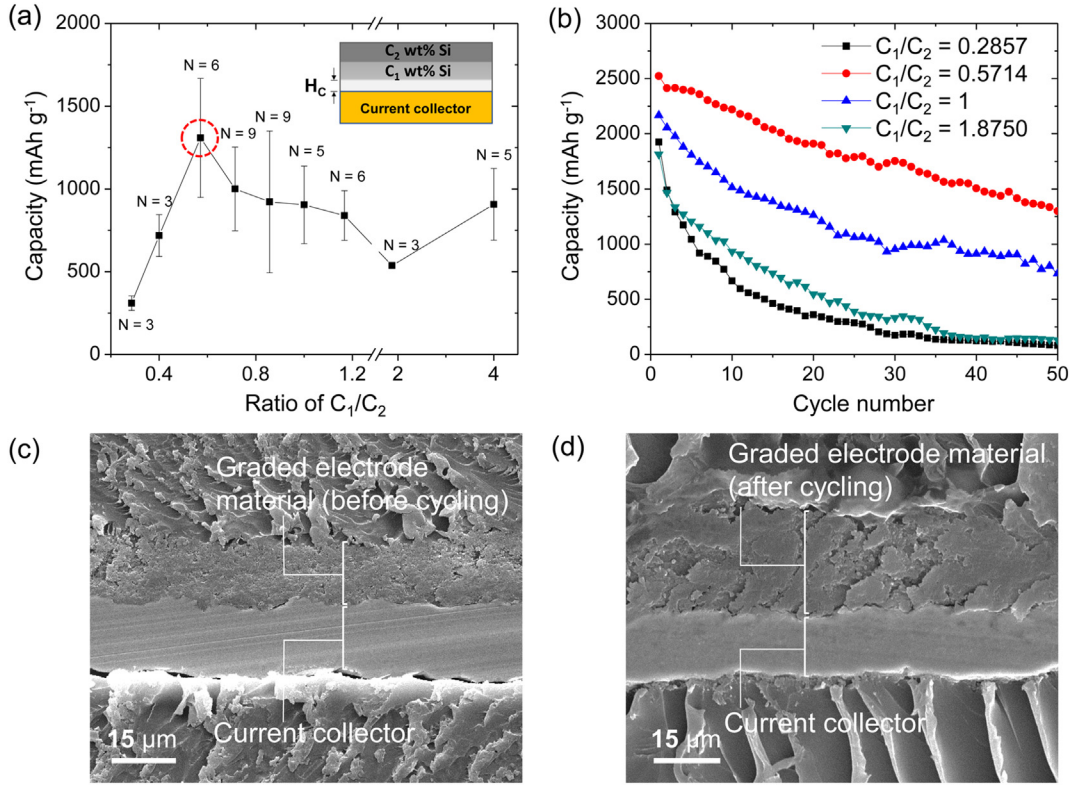

Fig. 6. (a) Variation of the capacity at the 20th cycle of three-layer graded electrodes with the ratio of C_1/C_2. *N* is the number of the tested cells and the error bar represents the standard deviation of the results obtained from *N* cells. Here, the thickness of the Si-free layer H_c is constantly equal to 25 μm. (b) The capacity (charge) of the three-layer graded electrodes with different C_1/C_2 during cycling test at a voltage between 0.01 V and 1.2 V vs. Li/Li^+ and a rate of 0.05 C. (c-d) SEM images of the cross-sections of the three-layer graded electrodes ($C_1/C_2 \cong 0.57$) before and after cycling (50 cycles).

4. Conclusion

The drastic volume change of Si during lithiation/delithiation processes leads to interfacial delamination between the current collector and the electrode materials, resulting in poor cyclability and low areal loading of active material in Si-based electrodes. In this paper, we tackled such delamination problem by reallocating the Si nanoparticles in space in a layer-graded way. The resulting graded electrodes exhibited much better electrochemical performance and higher utilizing efficiency of Si in comparison to the homogeneous controls containing the same amount of constituent materials. Structural optimization was carried out and the optimal structural designs of graded electrodes were found. Our approach is facile, low-cost and can be easily implemented by existing manufacturing techniques. Due to the limitation of the casting-based fabrication method, here we only considered the step-wise graded electrodes with limited (2–3) layers. It is believed that the performance of the electrode can be improved further if finer intervals of Si concentration or even continuous variation of Si concentration is applied. Such varying Si concentration may be fabricated using more sophisticated techniques such as additive manufacturing or direct ink writing [35–37]. Admittedly, our approach only aimed at the interfacial delamination problem, which is one of the factors causing the degradation of performance of LIB. A complete solution to the large-volume-change problem in Si-based electrode entails the synergy of multiple approaches [34,38–40] with the present one included.

CRediT authorship contribution statement

Zhenbin Guo: Investigation, Writing - original draft. **Limin Zhou:** Resources, Writing - review & editing. **Haimin Yao:** Conceptualization, Writing - review & editing, Funding acquisition, Supervision.

Acknowledgments

This work was supported by the National Natural Science Foundation of China (11772283), the General Research Fund (PolyU 152064/15E, PolyU 5293/13E) from Hong Kong RGC, and Centre of Excellence Scheme of the Hong Kong Polytechnic University (1-ZE30).

Data availability

All relevant data are included in the manuscript as Source Data; all other data are available from the corresponding authors upon reasonable request.

References

[1] T. Nagaura, K. Tozawa, Lithium-ion rechargeable battery, Prog. Batter. Solar Cells 9 (1990) 209–217.
[2] M. Armand, J.M. Tarascon, Building better batteries, Nature 451 (7179) (2008) 652–657.
[3] L. Croguennec, M.R. Palacin, Recent achievements on inorganic electrode materials for lithium-ion batteries, J. Am. Chem. Soc. 137 (9) (2015) 3140–3156.
[4] B.L. Ellis, K.T. Lee, L.F. Nazar, Positive electrode materials for Li-ion and Li-batteries, Chem. Mater. 22 (3) (2010) 691–714.
[5] J.M. Tarascon, M. Armand, Issues and challenges facing rechargeable lithium batteries, Nature 414 (6861) (2001) 359–367.
[6] J. Fan, T. Wang, C. Yu, B. Tu, Z. Jiang, D. Zhao, Ordered, nanostructured Tin-based oxides/carbon composite as the negative-electrode material for lithium-ion batteries, Adv. Mater. 16 (16) (2004) 1432–1436.
[7] S. Han, B. Jang, T. Kim, S.M. Oh, T. Hyeon, Simple synthesis of hollow tin dioxide microspheres and their application to lithium-ion battery anodes, Adv. Funct. Mater. 15 (11) (2005) 1845–1850.
[8] H. Wu, Y. Cui, Designing nanostructured Si anodes for high energy lithium ion batteries, Nano Today 7 (5) (2012) 414–429.
[9] N. Nitta, F. Wu, J.T. Lee, G. Yushin, Li-ion battery materials: present and future, Mater. Today 18 (5) (2015) 252–264.
[10] K. Feng, M. Li, W. Liu, A.G. Kashkooli, X. Xiao, M. Cai, Z. Chen, Silicon-based anodes for lithium-ion batteries: from fundamentals to practical applications, Small 14 (8) (2018), 1702737.
[11] N. Liu, Z. Lu, J. Zhao, M.T. McDowell, H.W. Lee, W. Zhao, Y. Cui, A pomegranate-inspired nanoscale design for large-volume-change lithium battery anodes, Nat. Nanotechnol. 9 (2014) 187–192.
[12] I. Kang, J. Jang, M.S. Kim, J.W. Park, J.H. Kim, Y.W. Cho, Nanostructured silicon/silicide/carbon composite anodes with controllable voids for Li-ion batteries, Mater. Des. 120 (2017) 230–237.
[13] X.H. Liu, L. Zhong, S. Huang, S.X. Mao, T. Zhu, J.Y. Huang, Size-dependent fracture of silicon nanoparticles during lithiation, ACS Nano 6 (2) (2012) 1522–1531.
[14] S.H. Ng, J. Wang, D. Wexler, K. Konstantinov, Z.P. Guo, H.K. Liu, Highly reversible lithium storage in spheroidal carbon-coated silicon nanocomposites as anodes for lithium-ion batteries, Angew. Chem. Int. Ed. 45 (41) (2006) 6896–6899.
[15] M.E. Stournara, Y. Qi, V.B. Shenoy, From ab initio calculations to multiscale design of Si/C core-shell particles for Li-ion anodes, Nano Lett. 14 (4) (2014) 2140–2149.
[16] W. Li, K. Cao, H. Wang, J. Liu, L. Zhou, H. Yao, Carbon coating may expedite the fracture of carbon-coated silicon core-shell nanoparticles during lithiation, Nanoscale 8 (9) (2016) 5254–5259.
[17] W. Li, Q. Wang, K. Cao, J. Tang, H. Wang, L. Zhou, H. Yao, Mechanics-based optimization of yolk-shell carbon-coated silicon nanoparticle as electrode materials for high-capacity lithium ion battery, Compos. Commun. 1 (2016) 1–5.
[18] N. Liu, H. Wu, M.T. McDowell, Y. Yao, C. Wang, Y. Cui, A yolk-shell design for stabilized and scalable Li-ion battery alloy anodes, Nano Lett. 12 (6) (2012) 3315–3321.
[19] X. Zhou, J. Tang, J. Yang, J. Xie, L. Ma, Silicon@carbon hollow core-shell heterostructures novel anode materials for lithium ion batteries, Electrochim. Acta 87 (2013) 663–668.
[20] Y. Yao, M.T. McDowell, I. Ryu, H. Wu, N. Liu, L. Hu, W.D. Nix, Y. Cui, Interconnected silicon hollow nanospheres for lithium-ion battery anodes with long cycle life, Nano Lett. 11 (7) (2011) 2949–2954.
[21] S. Suresh, Graded materials for resistance to contact deformation and damage, Science 292 (5526) (2001) 2447–2451.
[22] B. Kieback, A. Neubrand, H. Riedel, Processing techniques for functionally graded materials, Mater. Sci. Eng. A 362 (1–2) (2003) 81–106.
[23] J. Aboudi, M.J. Pindera, S.M. Arnold, Higher-order theory for functionally graded materials, Compos. Part B 30 (8) (1999) 777–832.
[24] H. Yao, H. Gao, Gibson-soil-like materials achieve flaw-tolerant adhesion, J. Comput. Theor. Nanosci. 7 (7) (2010) 1299–1305.
[25] C.Y. Huang, Y.L. Chen, Design and impact resistant analysis of functionally graded Al_2O_3-ZrO_2 ceramic composite, Mater. Des. 91 (2016) 294–305.
[26] H. Gao, B. Ji, I.L. Jäger, E. Arzt, P. Fratzl, Materials become insensitive to flaws at nanoscale: lessons from nature, Proc. Natl. Acad. Sci. U. S. A. 100 (10) (2003) 5597–5600.
[27] Z. Liu, M.A. Meyers, Z. Zhang, R.O. Ritchie, Functional gradients and heterogeneities in biological materials: design principles, functions, and bioinspired applications, Prog. Mater. Sci. 88 (2017) 467–498.
[28] B.J. Bruet, J. Song, M.C. Boyce, C. Ortiz, Materials design principles of ancient fish armour, Nat. Mater. 7 (9) (2008) 748–756.
[29] Y.K. Sun, S.T. Myung, B.C. Park, J. Prakash, I. Belharouak, K. Amine, High-energy cathode material for long-life and safe lithium batteries, Nat. Mater. 8 (2009) 320–324.
[30] K.B. Ghosh, J. Mukhopadhyay, R.N. Basu, Functionally graded doped lanthanum cobalt ferrite and ceria-based composite interlayers for advancing the performance stability in solid oxide fuel cell, J. Power Sources 328 (2016) 15–27.
[31] Y. Zhang, O.I. Malyi, Y. Tang, J. Wei, Z. Zhu, H. Xia, W. Li, J. Guo, X. Zhou, Z. Chen, Reducing the charge carrier transport barrier in functionally layer-graded electrodes, Angew. Chem. Int. Ed. 56 (47) (2017) 14847–14852.
[32] Q. Wei, X. Wang, X. Yang, B. Ju, B. Hu, H. Shu, W. Wen, M. Zhou, Y. Song, H. Wu, Spherical concentration-gradient $LiMn_{1.87}Ni_{0.13}O_4$ spinel as a high performance cathode for lithium ion batteries, J. Mater. Chem. A 1 (12) (2013) 4010–4016.
[33] G.M. Koenig Jr., I. Belharouak, H. Deng, Y.-K. Sun, K. Amine, Composition-tailored synthesis of gradient transition metal precursor particles for lithium-ion battery cathode materials, Chem. Mater. 23 (7) (2011) 1954–1963.
[34] L. Yue, L. Zhang, H. Zhong, Carboxymethyl chitosan: a new water-soluble binder for Si anode of Li-ion batteries, J. Power Sources 247 (2014) 327–331.
[35] K. Sun, T.S. Wei, B.Y. Ahn, J.Y. Seo, S.J. Dillon, J.A. Lewis, 3D printing of interdigitated Li-ion microbattery architectures, Adv. Mater. 25 (33) (2013) 4539–4543.
[36] L.T. Le, M.H. Ervin, H. Qiu, B.E. Fuchs, W.Y. Lee, Graphene supercapacitor electrodes fabricated by inkjet printing and thermal reduction of graphene oxide, Electrochem. Commun. 13 (4) (2011) 355–358.
[37] A.R. Studart, Additive manufacturing of biologically-inspired materials, Chem. Soc. Rev. 45 (2) (2016) 359–376.
[38] H. Wu, G. Chan, J.W. Choi, I. Ryu, Y. Yao, M.T. McDowell, S.W. Lee, A. Jackson, Y. Yang, L. Hu, Y. Cui, Stable cycling of double-walled silicon nanotube battery anodes through solid-electrolyte interphase control, Nat. Nanotechnol. 7 (5) (2012) 310–315.
[39] A. Magasinski, P. Dixon, B. Hertzberg, A. Kvit, J. Ayala, G. Yushin, High-performance lithium-ion anodes using a hierarchical bottom-up approach, Nat. Mater. 9 (4) (2010) 353–358.
[40] M.H. Park, M.G. Kim, J. Joo, K. Kim, J. Kim, S. Ahn, Y. Cui, J. Cho, Silicon nanotube battery anodes, Nano Lett. 9 (11) (2009) 3844–3847.